ACS SENSORS

pubs.acs.org/acssensors Article

Improving the Performance of Selective Solid-State Nanopore Sensing Using a Polyhistidine-Tagged Monovalent Streptavidin

Sara Abu Jalboush,[#] Ian D. Wadsworth,[#] Komal Sethi,[#] LeAnn C. Rogers, Thomas Hollis, and Adam R. Hall*

Cite This: https://doi.org/10.1021/acssensors.4c00200 Read Online

ACCESS | Metrics & More | Article Recommendations | Supporting Information

ABSTRACT: Solid-state (SS-) nanopore sensing has gained tremendous attention in recent years, but it has been constrained by its intrinsic lack of selectivity. To address this, we previously established a novel SS-nanopore assay that produces translocation signals only when a target biotinylated nucleic acid fragment binds to monovalent streptavidin (MS), a protein variant with a single high-affinity biotin-binding domain. While this approach has enabled selective quantification of diverse nucleic acid biomarkers, sensitivity enhancements are needed to improve the detection of low-abundance translational targets. Because the translocation dynamics that determine assay efficacy are largely governed by constituent charge characteristics, we here incorporate a polyhistidine-tagged MS (hMS) to alter the component detectability. We investigate the effects of buffer pH, salt concentration, and SS-nanopore diameter on the performance with the alternate reagent, achieve significant improvements in measurement sensitivity and selectivity, and expand the range of device dimensions viable for the assay. We used this improvement to detect as little as 1 nM miRNA spiked into human plasma. Overall, our findings improve the potential for broader applications of SS-nanopores in the quantitative analyses of molecular biomarkers.

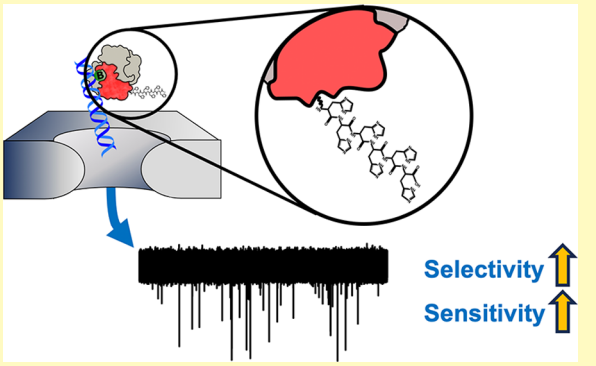

KEYWORDS: *solid-state nanopores, nucleic acids, monovalent streptavidin, amplification-free detection, selective detection, biomarkers*

Solid-state (SS-) nanopores are an emerging technology for biological sensing at the single-molecule level that has garnered interest due to remarkable sensitivity, versatility, robustness, and cost-effectiveness.[1,2] The device consists of a nanometer-scale aperture in a thin membrane that is positioned such that the pore is the only connection between two chambers of the ionic solution. When a voltage is applied across the membrane, a strong electric field is produced in the pore and an ionic current can be detected and monitored. Charged molecules introduced to one side of the membrane are subjected to electrical forces that translocate them through the pore and into the opposite chamber. During this translocation process, passing molecules produce transient blockades (i.e., events) in the ionic current that are typically used to report on aspects of the molecules themselves through event properties such as amplitude, duration, and rate. Over the past decade, the platform has been employed in the analysis of diverse (bio)molecules including DNA,[3−6] RNA,[7−9] proteins,[10−12] biomolecular complexes,[13−16] and small molecules.[17−19]

Despite the utility of SS-nanopore detection, a major limitation has been its lack of intrinsic selectivity; all translocating molecules produce signals and thus must be discriminated based on often subtle differences in event characteristics. This has been especially challenging for molecular disease biomarkers that are typically found in heterogeneous biological fluids, where molecules of similar sizes and physical properties may be present. To address this, multiple strategies have been implemented to improve event differentiation[3,20−25] and to preselect for target analytes.[10,26,27] Alternatively, we have developed an approach that achieves selectivity through molecular conjugation and steric interactions with the pore.[7,28−30] Our assay (Figure 1a) is composed of two elements: a short, biotin-labeled nucleic acid and a monovalent variant of the protein streptavidin (monovalent streptavidin, MS) that possesses only one active biotin-binding subunit.[31,32] When passing through a pore of an appropriate diameter individually, neither the nucleic acid nor the protein produces significant events due to their rapid threading, which cannot be detected easily by conventional electronics. However, when the two bind to form a nucleoprotein complex, its larger size interacts with the walls

Received: January 26, 2024
Revised: February 22, 2024
Accepted: February 27, 2024

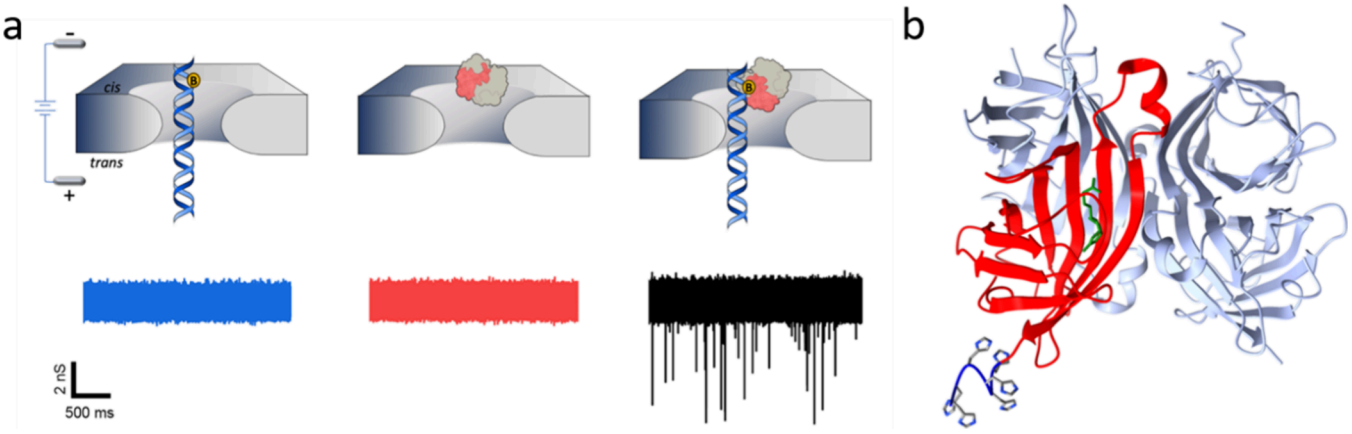

Figure 1. (a) Schematic (top) and example conductance traces (bottom) demonstrating the selective SS-nanopore assay. When translocated individually through an SS-nanopore, neither DNA (left) nor MS (center) yields significant events in the conductance trace (blue and red, respectively). When in complex (right), events are readily observed (black trace). (b) Structural representation of the polyhistidine-tagged MS. The streptavidin tetramer contains three inactive protomers (gray) and one active protomer (red) capable of binding biotin (green). The C-terminal polyhistidine tag on the active monomer is shown as a stick representation.

of the pore during translocation, slowing it to a resolvable speed.

The sensitivity and selectivity of our assay depend critically on many experimental parameters that have been explored systematically in prior studies to identify optimal conditions for assay performance.[28,33,34] One critical factor determining the dynamics of translocation is the charge associated with both the molecular components and the SS-nanopore itself. We recently investigated[30] the impact of modified salt conditions on our assay, thereby varying charge screening and influencing electrokinetics. While strong effects were observed, the systemic nature of buffer ionic concentration alone as an experimental variable limited our ability to modify charges independently; because all assay components are in contact with the buffer, it was not possible to vary the charge of any one component without affecting the others. Therefore, we reasoned that employing MS specifically with a less negative charge profile would alter the translocation dynamics of the nucleoprotein complex, potentially making it more detectable by reducing electrokinetic transport through the pore while maintaining stericity.

Here, we investigate this by utilizing an MS on which the conventional glutamate tag[32] has been replaced with a polyhistidine peptide tag (Figure 1b). Polyhistidine comprises a bulky ionizable side chain moiety in the form of an imidazole ring that is partially protonated at neutral pH, decreasing its net charge by about 6.5 $e-$ per protein relative to glutamic acid. Using this new reagent, we explore key experimental conditions, including buffer pH, buffer salt concentration, and SS-nanopore diameter, to determine their impacts on assay performance, ultimately demonstrating a significant improvement in both sensitivity and selectivity. Finally, we used these improvements to demonstrate enhanced translational biosensing with the assay by detecting a synthetic miRNA spiked into human plasma.

MATERIALS AND METHODS

Biomolecules. All synthetic DNAs and RNAs were purchased from Integrated DNA Technologies (Coralville, Iowa, USA). For assay optimization, monobiotinylated DNA oligo (60 nucleotides) with the sequence ATC AAC TGT TTC AGC CAC TGC TTC GCA GGC TGA CGT A**T**C TGA CGT GGT GCC AGC GAC GGA (where **T** indicates biotinylated thymine) was used to form double-stranded constructs via annealing with an unmodified complementary oligo. For human plasma measurements, a synthetic RNA oligo with the sequence UAC CCG UAA UCU UCA UAA UCC GAG was used, matching cel-miR-54, a 24 nt miRNA associated with *Caenorhabditis elegans* and not found in human specimens. A complement monobiotinylated DNA oligo probe (CTC GGA TTA **T**GA AGA TTA CGG GTA) was utilized as a probe to form RNA/DNA heteroduplex constructs.

Recombinant polyhistidine-tagged monovalent streptavidin (hMS) was produced in-house as a heterogeneous tetrameric variant of streptavidin containing one wild-type (WT) monomer with high-affinity biotin-binding capacity and three mutant (inactive) monomers.[31,32] The genes encoding the streptavidin^{WT} and streptavidin$^{N12A/S16D/S34A}$ proteins were each expressed as a fusion with maltose-binding protein (MBP) in a pET28 vector. The sequences included the rhinovirus 3C protease recognition site between the MBP and streptavidin to allow for cleavage and removal of the MBP. The streptavidin^{WT} sequence included a C-terminal polyhistidine sequence. WT and mutant fusion monomers were expressed independently in BL21* *Escherichia coli*. Each resulting fusion protein was then captured separately on an amylose resin column (New England Biolabs, Ipswich, Massachusetts, USA), washed, and eluted. The fusion proteins were then cleaved by glutathione-S-transferase-tagged (GST) PreScission Protease (GenScript, Piscataway, New Jersey, USA), separating the streptavidin from MBP. Following cleavage of the fusion protein, GST-PreScission Protease was removed by a glutathione resin column (New England Biolabs, Ipswich, Massachusetts, USA) to produce stocks of mutant and WT proteins. The WT and mutant streptavidin proteins were then mixed at a molar ratio of 1:4 and denatured in 8 M guanidinium hydrochloride (pH 1.5) (Sigma-Aldrich, Saint Louis, Missouri, USA) at 50 °C for 1 h. The denatured protein mixture was added dropwise into cold 1× PBS under constant stirring and then left stirring overnight to induce protein refolding. The MBP was then removed by passing the protein mixture over an amylose resin column a second time, after which MS tetramer was isolated and purified using a HisTrap HP nickel column (Cytiva, Marlborough, Massachusetts, USA). Finally, hMS was concentrated by a spin column (Sartorius, Göttingen, Germany). hMS protein purity was confirmed by SDS-PAGE, and its activity was verified by electromobility shift assay (Supplementary Figure S1).

SS-Nanopore Measurements. SS-nanopores were fabricated with a helium-ion milling (HIM) technique described elsewhere[35] in 20 nm silicon nitride (SiNx) membranes supported by a silicon chip (4.4 × 4.4 mm). Prior to measurements, each device was first exposed to 10 W air plasma (Harrick Plasma, Ithaca, New York, USA) for 2

https://doi.org/10.1021/acssensors.4c00200
ACS Sens. XXXX, XXX, XXX−XXX

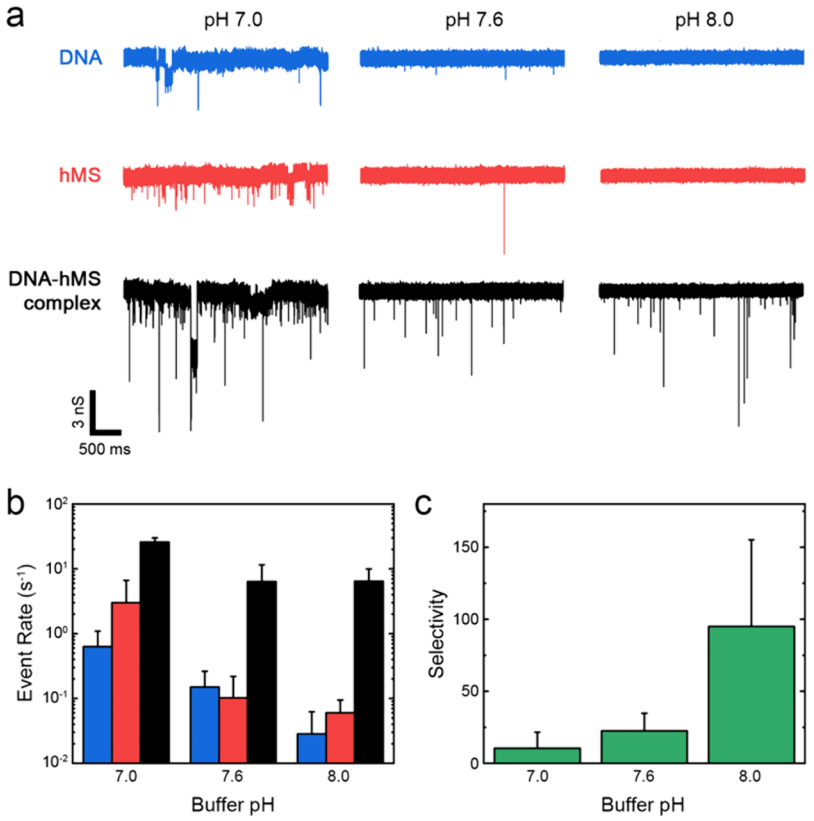

Figure 2. (a) Representative conductance traces for DNA only (blue), hMS only (red), and the DNA−hMS complex (black) at (l−r) pH 7.0, 7.6, and 8.0. (b) Translocation event rates ($n \geq 3$) measured for DNA only (blue), hMS only (red), and the DNA−hMS complex (black) for all examined pH conditions. (c) Measured selectivity ($n \geq 3$) for all examined pH conditions. Error bars represent the standard deviation of the measurements.

min on each side and then mounted in a custom flow cell fabricated with a commercial 3D printer (Carbon, Redwood City, California, USA). Both sides of the chip were then contacted with measurement buffer consisting of 10 mM Tris-base, 1 mM EDTA, and NaCl concentration and pH as described in the text. Ag/AgCl electrodes introduced to each reservoir were used to apply voltage and measure ionic current by using a commercial patch-clamp amplifier (Axopatch 200B, Axon Instruments, San Jose, California, USA). The diameter d_{pore} of a SS-nanopore device was determined from its open-pore current−voltage (I−V) response using the expression.[26]

$$I = V\sigma\left[\left(\frac{4L}{d_{pore}^2}\right) + \left(\frac{1}{d_{pore}}\right)\right]^{-1}$$

where I is the current, V is the applied voltage, σ is the bulk conductivity of the solution, and L is the effective length of the pore (considered to be 1/3 total membrane thickness following previous reports[26]).

All of the presented measurements were performed under a 300 mV applied bias. Translocation data were collected at 200 kHz with a 100 kHz Bessel filter and recorded using in-house data acquisition software (LabVIEW National Instruments, Austin, Texas, USA). An additional 10 kHz low-pass filter was applied digitally during the analysis. Transient reductions in measured SS-nanopore conductance were considered only if their durations were between 25 and 2500 μs, and their amplitudes were at least 4.5 standard deviations from baseline noise. Data were recorded in discrete 3.2 s segments, from which the average rate was calculated. All measurements were performed on 100 nM DNA, 500 nM hMS, or a mixture of the two incubated for 30 min at room temperature to produce the DNA−hMS complex.

For pH optimization, measurements were performed on SS-nanopores with diameters between 7.3 and 10.1 nm. At least four separate nanopores were utilized for each condition. For salt concentration optimization, measurements were performed on SS-nanopores with diameters between 7.7 and 10.6 nm. Analysis under each condition was repeated using three different SS-nanopores except for 1.0 M (n = 4) and 1.25 M (n = 5) NaCl. For diameter dependence measurements, 14 independent SS-nanopores were employed with diameters from 7.3 to 23.1 nm. All measurements were performed for at least 5 min except for pH 7.0 due to instability and clogging.

miRNA Quantification. Whole blood acquired from a healthy human subject (Atrium Wake Forest Baptist protocol number IRB00039804) was immediately processed by centrifugation at 1500 × g at 4 °C for 15 min. Separated plasma was stored at −80 °C prior to use. An miRNeasy Serum/Plasma Advanced Kit (Qiagen, Germantown, Maryland, USA) was used to isolate small RNA (including miRNA) from 200 μL of plasma. Synthetic cel-miR-54 miRNA (described above) was spiked into the plasma at concentrations of 1, 10, or 100 nM after the addition of the protein precipitate buffer (kit buffer "RPP") to ensure the stability of the bare synthetic RNA. Purification was performed according to the manufacturer's instructions but with the final elution step conducted twice to maximize recovery.[36] RNA isolate from an unspiked plasma aliquot was also acquired using the same procedure and used as a negative control. After isolation, a biotinylated DNA complement probe (100 nM) was added to all isolates and heated to 95 °C for 10 min and then cooled to 39 °C over 2 h to promote annealing to miRNA oligos. hMS was then added (500 nM) to bind to the biotinylated DNA and form the RNA/DNA heteroduplex−hMS complex, where spike-in was present. Finally, the samples were measured with a single SS-nanopore for consistency (beginning

https://doi.org/10.1021/acssensors.4c00200
ACS Sens. XXXX, XXX, XXX−XXX

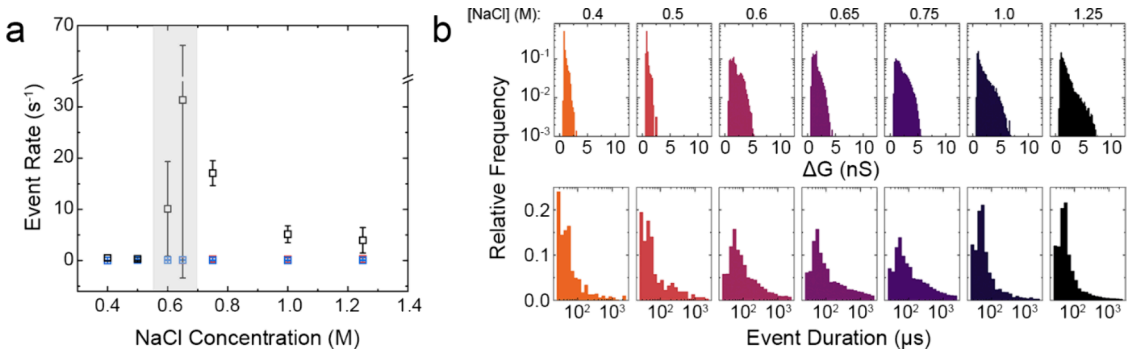

Figure 3. (a) Translocation event rate ($n \geq 3$) for DNA only (blue), hMS only (red), and the DNA−hMS complex (black) as a function of buffer NaCl concentration. The shaded region indicates a transitionary region, where measured rates were highly variable. Error bars represent the standard deviation of measurements taken on at least three independent SS-nanopore devices. (b) Conductance change (ΔG, top) and event duration (bottom) histograms for measured DNA-hMS events across all NaCl (l−r: n = 711, 313, 8724, 15391, 17383, 7344, and 7332).

diameter 9.4 nm and final diameter 10.5 nm), utilizing the experimental conditions optimized in this study.

RESULTS AND DISCUSSION

Buffer pH can influence the translocation dynamics of biomolecules through SS-nanopores[37] by modifying the surface charges of all components in contact with the buffer or in extreme conditions by altering the molecular structure.[38] These changes can impact the speed and direction of translocation,[39] the molecular capture rate, and the level of interaction between the pore surface and target molecules. Consequently, we initially sought to probe the effect of buffer pH on the performance of the assay incorporating hMS. For this purpose, we performed a series of SS-nanopore measurements across a pH range of 7.0 to 8.0, chosen to be above the isoelectric points (pI) of all assay components to ensure their net negative charge: the pI for both the SS-nanopore surface[39] and the double-stranded DNA (dsDNA)[40] was taken to be ∼5.0 from prior literature while the pI of the hMS was 6.0 as calculated[41] using the pK values[42] of all amino acids in its sequence, including the polyhistidine tag itself.

For each pH condition, analyses were conducted on at least four independent SS-nanopore devices and in standard 1 M NaCl. Measurements included DNA only (using 60 bp dsDNA with a single biotin as a standard; 100 nM), hMS only (500 nM), and finally an incubated mixture of the two constituents to form a DNA−hMS complex. Considering representative conductance traces for all investigated conditions (Figure 2a), more translocation signals per unit time were observed at low pH. Quantitative analyses confirmed this, showing that the measured event rates for all three groups reduced as pH increased (Figure 2b). There are several possible explanations for this observation. First, the progressively more negative net charge of the molecular constituents as pH is increased above the pI could have had the effect of reducing event durations due to a higher electrophoretic driving force, making translocations more difficult to resolve and thereby reducing the apparent event rate. Indeed, like other proteins, the charge of streptavidin is known to change significantly with pH[39,43]; even a simple summation of all amino acid pK_a values in hMS suggests that a twofold increase in net negative charge could be expected between pH 7.0 and 8.0. However, the charge of DNA has been shown to be nearly invariant across the same range[44,45] and the observed rate for DNA alone in our measurements (Figure 2b) decreased by almost the same amount as hMS (Figure 2b) across the pH window. In addition, the charge of the nanopore surface itself has been shown experimentally to become more negative across this pH range as well.[39,46] The resulting electroosmotic flow would slow translocation speeds, which could be expected to make them more detectable and increase the measured event rate, counter to our observation. Consequently, we consider these electrodynamic effects to be unlikely explanations for the data.

As a second possibility, the baseline noise of the conductance could have increased with pH and made events harder to discern from the noise floor, resulting in a decrease in measured rate. However, we found that the baseline noise (standard deviation) of the baseline actually decreased with pH (Supplementary Figure S2), in agreement with a recent work[47] that showed that the electrical noise in SS-nanopores is greatest at the pI. Therefore, this is not considered an adequate rationalization for the observed results.

Instead, we suggest that the additional events recorded at low pH were caused by more frequent and longer-lasting stochastic collisions between the biomolecules and the silicon nitride surface, driven by weaker charge differentials under those conditions. We have shown previously[48] that apparent events can manifest from transient interactions with the sensing region near the SS-nanopore. These events tend to be low-amplitude due to their partial blockage of the pore and can occur even without molecular translocation. Examining the measured conductance traces and event properties (Supplementary Figure S3) closely, we observed that the low-amplitude events with a broad range of durations found at pH 7.0 were less abundant as the pH was increased. We also noted a difference in stability across conditions, with a low-frequency variation in the baseline conductance at pH 7.0 that made measurements more difficult to perform, suggesting strong and unpredictable interactions. At higher pH where these interactions were less significant and nontranslocative events were reduced, very few signals for either the DNA or the hMS alone were observed even while the nucleoprotein complex was still detected readily. This effect could be quantified through assay selectivity, defined as the ratio of the nucleoprotein complex event rate to the combined rates of the independent DNA and hMS constituents.[30] We found that selectivity increased significantly with pH (Figure 2c), reaching >100 at pH 8.0—more than twice the value that had been achieved with prior MS under similar conditions.[30] Consequently, pH 8.0 was identified as being optimal for subsequent measurements.

https://doi.org/10.1021/acssensors.4c00200
ACS Sens. XXXX, XXX, XXX−XXX

Having established a buffer pH condition to achieve enhanced assay selectivity, we next sought to optimize the measurement sensitivity by varying salt concentration. Ionic strength is known to influence both event properties and analyte translocation dynamics in SS-nanopore measurements.[23,49,50] Because the source of selectivity for our approach in particular is the relative detectability of the different molecular components, salt conditions have also been shown[30] to impact its efficacy. High ionic strength has competing effects in the assay, making events easier to resolve by increasing event amplitude and duration[49] and decreasing baseline noise[51,52] but also decreasing their frequency by a reducing electrophoretic driving force via efficient charge screening. Because these effects are influenced by molecular charge, we expected that our incorporation of hMS could impact the assay performance. To investigate this, we conducted another series of measurements on DNA alone, hMS alone, and DNA−hMS complexes at the same molecular concentrations as above and at a pH of 8.0 but across a broad range of NaCl from 0.4 to 1.25 M.

We first observed that both DNA and hMS alone maintained a low event rate at or near zero, with no significant variation across the entire NaCl range (Figure 3a). Especially for the lower concentrations, this matched expectations; since events for both constituents were essentially undetectable at 1 M NaCl (*c.f.,* Figure 3a), reducing the salt concentration further would only make their detection more challenging due to a reduced signal-to-noise ratio (SNR) even if the total number of translocating molecules increased. However, the rate measured for the DNA−hMS complex varied considerably across the same span (Figure 3a). The highest concentration investigated (1.25 M NaCl) yielded a relatively low event rate. Here, most or all translocating nucleoprotein complexes were detectable but relatively few translocations occurred due to efficient counterion screening. As the salt concentration was reduced, we observed a concomitant increase in the measured rate. We interpreted this behavior to result from an increasing capture rate induced by weakened charge screening of the nucleoprotein complex due to reduced counterion availability. This appeared to be the dominant effect, even though SNR and event duration were both expected to decline over the same range, thus making low-amplitude and fast events harder to resolve. For example, event amplitudes were found to decrease progressively with decreasing salt concentration (Figure 3b, top; Supplementary Figure S4), confirming the SNR reduction. For event duration, while similar analyses initially seemed to show an unexpected increase in dwell time at low salt conditions where the DNA−hMS complex was efficiently detected (Figure 3b, bottom), the observed shifts actually resulted from fast events that became increasingly indistinguishable from the noise under low SNR conditions. We postulated that salt-dependent differences in DNA−hMS complex orientation may have been a main factor in translocation event temporal detectability.

Upon reducing the NaCl concentration to 0.65 and then 0.6 M, we found a transitional state (Figure 3a, shaded region) in which measured event rates were found to be highly variable between replicates. This behavior was attributed to a significant portion of events being barely detectable above the noise and consequently yielding rates that depended on small differences between independent SS-nanopores. Additionally, conductance traces measured at these conditions were unstable (Supplementary Figure S5), possibly suggesting increased interactions between the DNA−hMS complex and the pore walls due to weak counterion screening. These interactions may have impacted event detection randomly, contributing to the rate variability. At low salt concentrations of 0.5 and 0.4 M, DNA-hMS event rates were very low and were not distinguishable from those of the DNA or hMS alone due to the low SNR that prevented any events from being resolved.

We note that our results with hMS had several key similarities with past measurements using an MS with higher net charge.[30] For example, prior data also indicated the emergence of detectable nucleoprotein events at approximately 0.6 M NaCl because this detection threshold is driven by the noise of the measurement apparatus rather than molecular properties like charge. Additionally, the event rate at the high salt limit measured here ($4.0 \pm 2.5\ s^{-1}$) is close to the prior study ($4.6 \pm 0.6\ s^{-1}$), demonstrating that the net charges of the constructs at counterion saturation are comparable. However, the rate maximization observed here at intermediate salt concentrations was unique to the DNA−hMS complex. Whereas the prior construct was saturated with counterions at all NaCl concentrations above approximately 0.6 M, the reduced negative charge associated with the polyhistidine tag here afforded our present measurements a greater window of detectability where partial screening enabled the capture rate enhancement to be resolved. As a result, 0.75 M NaCl yielded an approximately threefold higher sensitivity than reported previously[30] and considerably higher selectivity than past results at the same salt concentration using glutamate-tagged MS.[30] We note that while the selectivity observed here (∼55) is somewhat less than that reported above for 1 M NaCl (∼100, see Figure 2c), this is a consequence of a very slight increase in constituent rate and is still robust.

Because steric interactions drive the discriminatory detection in our assay, SS-nanopore diameter is another critical factor affecting selectivity.[34] Pore diameters that closely match the size of the nucleoprotein complex generally increase the probability of interactions, thereby yielding the highest possible event rates, in contrast to larger-diameter pores that permit more rapid translocations to go undetected. Indeed, small differences in diameter can partially account for the variability that has been observed between measurements and can, in principle, be corrected for through a quantitative understanding of its dependence. While pore diameter dependence has been measured for our assay previously,[34] its impact on the improved performance realized with hMS must be determined explicitly. To achieve this, we finally probed DNA, hMS, and DNA−hMS complex using a series of 14 independent SS-nanopores across the diameter range of 7.3 to 23.1 nm. Molecular concentrations were identical to those above, and optimized buffer conditions of pH 8.0 and 0.75 M NaCl were used for all measurements.

Considering DNA−hMS complex event rates and summed hMS and DNA event rates separately (Figure 4b), we confirmed both that events associated with the constituents remained consistently low and that nucleoprotein events decreased drastically with an increasing pore diameter (Figure 4a,b). The reduction was well-described by a semilog fit (linear on a semilog scale, Figure 4b, black line), similar to past results.[34] For the smallest SS-nanopore studied here (7.3 nm), we observed significant transient clogging of the device compared to larger-diameter pores (Supplementary Figure S6), demonstrating that steric hindrance was too strong under

https://doi.org/10.1021/acssensors.4c00200
ACS Sens. XXXX, XXX, XXX−XXX

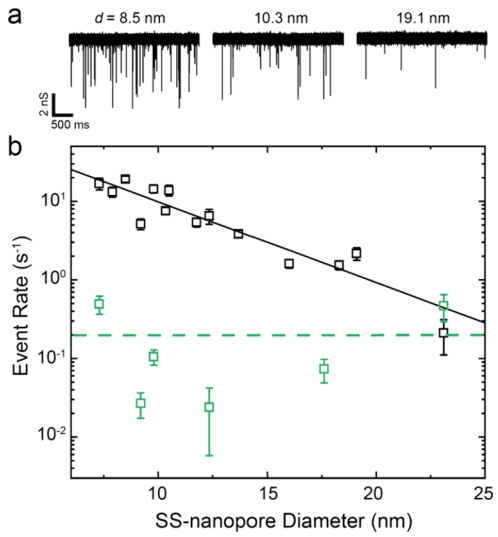

Figure 4. (a) Example conductance traces for DNA−hMS measured with SS-nanopores of diameters 8.5 (left), 10.3 (center), and 19.1 nm (right). (b) Event rate as a function of SS-nanopore diameter for the DNA−hMS complex (black) and the summation of the DNA and hMS independently (green). Error bars represent the standard deviation of the measurements. The black line is a semilog fit to the DNA−hMS data. The dashed green line is the mean value of the summed constituent event rates.

that condition to enable smooth translocations. From this, we concluded that 7.5 nm was the minimum diameter possible for assay implementation, correlating with the dimensions of the nucleoprotein complex and with our prior findings.[7] As in prior studies, fewer resolvable translocations were observed for large-diameter SS-nanopores because of limited interaction with the pore walls. However, the enhanced sensitivity achieved here with optimized conditions still afforded a wide dynamic range for the assay; the DNA−hMS complex yielded an event rate that was more than one order of magnitude higher than the mean rate of the summed constituents up to approximately 16 nm, relieving prior constraints[34] that limited the assay to pores below 10 nm. This ultimately reduces the variability of results obtained with SS-nanopores of similar dimensions and facilitates the easier fabrication of devices viable for the application.

Having optimized measurement conditions for improved sensitivity and selectivity with the hMS reagent, we finally sought to leverage these improvements to enhance biosensing with the SS-nanopore assay. To do this, we investigated the quantitative measurement of miRNA, an analysis that typically requires specialized methods of reverse transcription quantitative polymerase chain reaction (RT-qPCR)[53−55] to perform due to the small size (20−25 nt) of the target. We have previously[7] demonstrated that specific miRNA sequences can be detected using an adaptation of our selective assay in which a biotinylated single-strand (ss) DNA probe and MS are introduced to solution and translocation events are resolved only if the probe hybridizes with its complementary target; discrimination arises from the observation that ssDNA-MS does not produce events in contrast to duplex nucleoprotein complexes, as described above. In our past work, we established this approach with miRNA in a clean buffer with no interfering molecules. Here, we challenge our assay by discriminating an miRNA spiked into human plasma containing a mixture of native, off-target nucleic acids.

For our measurements, four aliquots of human plasma were prepared (Figure 5a): one kept native and three spiked with a

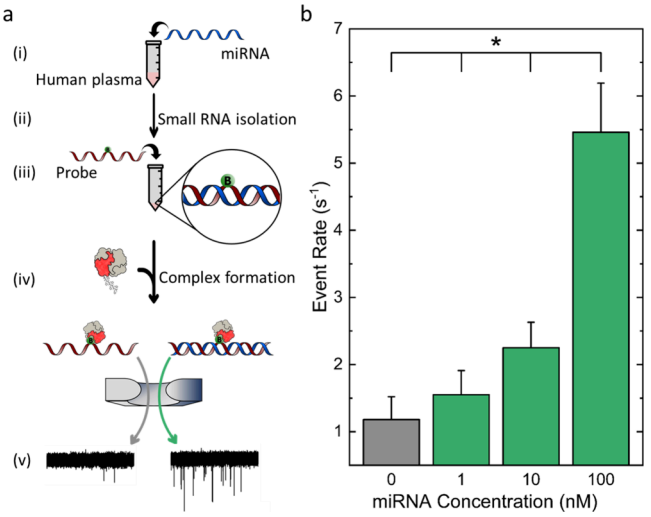

Figure 5. (a) Schematic of workflow for miRNA spike-in and analysis, showing (i) spike-in of miRNA (blue) in human plasma, (ii) isolation of small RNAs (including miRNA), (iii) addition of a biotinylated ssDNA complementary probe (red) for heteroduplex formation, (iv) addition of hMS to form nucleoprotein complexes, and (v) SS-nanopore analysis. Off-target and background RNAs not shown for clarity. (b) Nanopore event rates measured across a range of miRNA spike-in concentrations. Error bars represent the standard deviation of the segmented measurements (see Materials and Methods for details; segment counts were (l−r) 108, 138, 164, and 121). All concentrations differed significantly (*$p < 0.001$) as determined by ANOVA and Tukey's HSD post hoc analysis.

synthetic 24 nt miRNA (see Materials and Methods) at concentrations of 1, 10, and 100 nM. Small RNAs (including miRNAs) were then isolated from the samples independently, and a biotinylated ssDNA probe with a sequence complementary to the miRNA spike-in was added to each at 100 nM concentrations to enable the formation of RNA/DNA heteroduplexes. Finally, hMS was added to the aliquots as above (500 nM) to form complexes with all biotinylated constructs and the samples were analyzed by SS-nanopore using optimal conditions (0.75 M NaCl, pH 8.0, 9.4 nm beginning pore diameter). The event rate for the native, unspiked sample (Figure 5b, gray) was low but significant at 1.2 ± 0.3 s^{-1}. This reflected the contribution of unhybridized probe−hMS complexes, as well as translocations of off-target miRNAs and other larger RNAs from the plasma. Because all of these components were present under all conditions and defined a consistent background signal, the event rate from plasma alone (no probe or hMS) had no direct impact on discriminatory power and was not measured here. Subsequent identical measurements of the spiked samples produced changes in event rate (Figure 5b, green; Supplementary Figure S7), yielding values of 5.5 ± 0.7 s^{-1} (100 nM), 2.3 ± 0.4 s^{-1} (10 nM), and 1.6 ± 0.4 s^{-1} (1 nM). The observed concentration dependence not only demonstrated the capacity of the hMS-optimized assay to detect a sequence-specific miRNA biomarker in complex biofluid but also suggested its ability to quantify it across a broad range of concentrations. In prior *in vitro* measurements[7] using an identical measurement procedure but with a conventional glutamate-tagged MS, we resolved only down to 10 nM miRNA even with no

https://doi.org/10.1021/acssensors.4c00200
ACS Sens. XXXX, XXX, XXX−XXX

background molecules. Critically, event rates for all concentrations investigated here were significantly greater than the unspiked control down to at least 1 nM, signifying that the hMS reagent and optimized measurement conditions yielded significant improvements in our assay performance and highlighting its translational potential.

CONCLUSIONS

In total, we have examined here the performance of a selective SS-nanopore assay after integrating hMS, an MS featuring a polyhistidine tag that yields a net negative charge lower than those of previous versions of the protein. Increasing the pH of the buffer decreased noise levels in the measurement and resulted in an increased number of true events as well as a minimization of nontranslocative signals. Although this decreased the overall measured event rate, it markedly enhanced the selectivity of the assay markedly. Subsequent optimization of the salt concentration in the measurement buffer enhanced the detection of low-amplitude events and significantly enhanced the sensitivity of our assay while maintaining high selectivity. Assay performance was evaluated across a range of SS-nanopore diameters, demonstrating a broad dynamic range of approximately 7.5 to 16 nm. Finally, we used the optimized conditions to enhance miRNA assessment in human plasma, resolving concentrations as little as 1 nM above baseline without amplification, or an order of magnitude better than achieved previously.[7] Together, these findings establish the capacity of the hMS reagent to improve the selective SS-nanopore assay significantly, strengthening its value for quantitative analyses of molecular biomarkers that include miRNAs, conserved pathogen sequences, and DNA epigenetic modifications and base lesions. Ultimately, our findings enhance the translational value of the platform.

ASSOCIATED CONTENT

Supporting Information

The Supporting Information is available free of charge at https://pubs.acs.org/doi/10.1021/acssensors.4c00200.

SDS-PAGE and EMSA gel images for hMS verification, SS-nanopore baseline noise analyses, translocation event characteristics across pH and NaCl conditions, and representative conductance traces (PDF)

AUTHOR INFORMATION

Corresponding Author

Adam R. Hall − *Virginia Tech-Wake Forest University School of Biomedical Engineering and Sciences, Wake Forest School of Medicine, Winston-Salem, North Carolina 27101, United States; Comprehensive Cancer Center, Wake Forest School of Medicine, Winston-Salem, North Carolina 27157, United States;* orcid.org/0000-0003-2053-6075; Email: arhall@wakehealth.edu

Authors

Sara Abu Jalboush − *Department of Cancer Biology, Wake Forest School of Medicine, Winston-Salem, North Carolina 27157, United States;* orcid.org/0009-0009-9913-4175

Ian D. Wadsworth − *Virginia Tech-Wake Forest University School of Biomedical Engineering and Sciences, Wake Forest School of Medicine, Winston-Salem, North Carolina 27101, United States*

Komal Sethi − *Virginia Tech-Wake Forest University School of Biomedical Engineering and Sciences, Wake Forest School of Medicine, Winston-Salem, North Carolina 27101, United States*

LeAnn C. Rogers − *Department of Biochemistry, Wake Forest School of Medicine, Winston-Salem, North Carolina 27157, United States*

Thomas Hollis − *Department of Biochemistry, Wake Forest School of Medicine, Winston-Salem, North Carolina 27157, United States;* orcid.org/0000-0002-4996-6346

Complete contact information is available at: https://pubs.acs.org/10.1021/acssensors.4c00200

Author Contributions

#S.A.J., I.D.W., and K.S. contributed equally to this work.

Notes

The authors declare no competing financial interest.

ACKNOWLEDGMENTS

This project was supported by NIH awards R21CA193067, R33CA246448, and P41EB020594 (A.R.H.). SS-nanopore fabrication was performed at the Rutgers University Laboratory for Surface Modification.

REFERENCES

(1) Howorka, S.; Siwy, Z. Nanopore Analytics: Sensing of Single Molecules. *Chem. Soc. Rev.* **2009**, *38* (8), 2360−2384.

(2) Haque, F.; Li, J.; Wu, H.-C.; Liang, X.-J.; Guo, P. Solid-State and Biological Nanopore for Real-Time Sensing of Single Chemical and Sequencing of DNA. *Nano Today* **2013**, *8* (1), 56−74.

(3) Wanunu, M.; Sutin, J.; McNally, B.; Chow, A.; Meller, A. DNA Translocation Governed by Interactions with Solid-State Nanopores. *Biophys. J.* **2008**, *95* (10), 4716−4725.

(4) Li, J.; Gershow, M.; Stein, D.; Brandin, E.; Golovchenko, J. A. DNA Molecules and Configurations in a Solid-State Nanopore Microscope. *Nat. Mater.* **2003**, *2* (9), 611−615.

(5) Heng, J. B.; Aksimentiev, A.; Ho, C.; Marks, P.; Grinkova, Y. V.; Sligar, S.; Schulten, K.; Timp, G. Stretching DNA Using the Electric Field in a Synthetic Nanopore. *Nano Lett.* **2005**, *5* (10), 1883−1888.

(6) Fologea, D.; Brandin, E.; Uplinger, J.; Branton, D.; Li, J. DNA Conformation and Base Number Simultaneously Determined in a Nanopore. *Electrophoresis* **2007**, *28* (18), 3186−3192.

(7) Zahid, O. K.; Wang, F.; Ruzicka, J. A.; Taylor, E. W.; Hall, A. R. Sequence-Specific Recognition of microRNAs and Other Short Nucleic Acids with Solid-State Nanopores. *Nano Lett.* **2016**, *16* (3), 2033−2039.

(8) Yan, H.; Weng, T.; Zhu, L.; Tang, P.; Zhang, Z.; Zhang, P.; Wang, D.; Lu, Z. Central Limit Theorem-Based Analysis Method for MicroRNA Detection with Solid-State Nanopores. *ACS Applied Bio Materials* **2021**, *4* (8), 6394−6403.

(9) Henley, R. Y.; Carson, S.; Wanunu, M. Studies of RNA Sequence and Structure Using Nanopores. *Progress in molecular biology and translational science* **2016**, *139*, 73−99.

(10) Rivas, F.; DeAngelis, P. L.; Rahbar, E.; Hall, A. R. Optimizing the Sensitivity and Resolution of Hyaluronan Analysis with Solid-State Nanopores. *Sci. Rep.* **2022**, *12* (1), 4469.

(11) Fologea, D.; Ledden, B.; McNabb, D. S.; Li, J. Electrical Characterization of Protein Molecules by a Solid-State Nanopore. *Appl. Phys. Letters* **2007**, *91* (5), No. 053901.

(12) Plesa, C.; Kowalczyk, S. W.; Zinsmeester, R.; Grosberg, A. Y.; Rabin, Y.; Dekker, C. Fast Translocation of Proteins through Solid State Nanopores. *Nano Lett.* **2013**, *13* (2), 658−663.

(13) Han, A.; Creus, M.; Schurmann, G.; Linder, V.; Ward, T. R.; De Rooij, N. F.; Staufer, U. Label-Free Detection of Single Protein Molecules and Protein− Protein Interactions Using Synthetic Nanopores. *Analytical chemistry* **2008**, *80* (12), 4651−4658.

(14) Smeets, R.; Kowalczyk, S. W.; Hall, A.; Dekker, N.; Dekker, C. Translocation of RecA-Coated Double-Stranded DNA through Solid-State Nanopores. *Nano Lett.* **2009**, *9* (9), 3089−3095.
(15) Squires, A.; Atas, E.; Meller, A. Nanopore Sensing of Individual Transcription Factors Bound to DNA. *Sci. Rep.* **2015**, *5* (1), 11643.
(16) Yu, J.-S.; Lim, M.-C.; Huynh, D. T. N.; Kim, H.-J.; Kim, H.-M.; Kim, Y.-R.; Kim, K.-B. Identifying the Location of a Single Protein along the DNA Strand Using Solid-State Nanopores. *ACS Nano* **2015**, *9* (5), 5289−5298.
(17) Kwak, D.; Chae, H.; Lee, M.; Ha, J.; Goyal, G.; Kim, M. J.; Kim, K.; Chi, S. Probing the Small-molecule Inhibition of an Anticancer Therapeutic Protein-protein Interaction Using a Solid-state Nanopore. *Angew. Chem., Int. Ed.* **2016**, *55* (19), 5713−5717.
(18) Lee, S. B.; Mitchell, D. T.; Trofin, L.; Nevanen, T. K.; Soderlund, H.; Martin, C. R. Antibody-Based Bio-Nanotube Membranes for Enantiomeric Drug Separations. *Science* **2002**, *296* (5576), 2198−2200.
(19) Tsutsui, M.; Taniguchi, M.; Yokota, K.; Kawai, T. Identifying Single Nucleotides by Tunnelling Current. *Nature Nanotechnol.* **2010**, *5* (4), 286−290.
(20) Yang, L.; Hu, J.; Li, M.; Xu, M.; Gu, Z. Solid-state Nanopores: Chemical Modifications, Interactions, and Functionalities. *Chem. - Asian J.* **2022**, *17* (22), No. e202200775.
(21) Wang, L.; Wang, H.; Chen, X.; Zhou, S.; Wang, Y.; Guan, X. Chemistry Solutions to Facilitate Nanopore Detection and Analysis. *Biosens. Bioelectron.* **2022**, *213*, No. 114448.
(22) Lee, K.; Park, K.-B.; Kim, H.-J.; Yu, J.-S.; Chae, H.; Kim, H.-M.; Kim, K.-B. Recent Progress in Solid-State Nanopores. *Adv. Mater.* **2018**, *30* (42), No. 1704680.
(23) Sha, J.; Shi, H.; Zhang, Y.; Chen, C.; Liu, L.; Chen, Y. Salt Gradient Improving Signal-to-Noise Ratio in Solid-State Nanopore. *ACS Sens.* **2017**, *2* (4), 506−512.
(24) Fologea, D.; Uplinger, J.; Thomas, B.; McNabb, D. S.; Li, J. Slowing DNA Translocation in a Solid-State Nanopore. *Nano Lett.* **2005**, *5* (9), 1734−1737.
(25) Tang, H.; Wang, H.; Yang, C.; Zhao, D.; Qian, Y.; Li, Y. Nanopore-Based Strategy for Selective Detection of Single Carcinoembryonic Antigen (CEA) Molecules. *Anal. Chem.* **2020**, *92* (4), 3042−3049.
(26) Wanunu, M.; Dadosh, T.; Ray, V.; Jin, J.; McReynolds, L.; Drndić, M. Rapid Electronic Detection of Probe-Specific microRNAs Using Thin Nanopore Sensors. *Nat. Nanotechnol.* **2010**, *5* (11), 807−814.
(27) Wang, H.; Tang, H.; Yang, C.; Li, Y. Selective Single Molecule Nanopore Sensing of microRNA Using PNA Functionalized Magnetic Core−Shell Fe3O4−Au Nanoparticles. *Anal. Chem.* **2019**, *91* (12), 7965−7970.
(28) Wang, F.; Zahid, O. K.; Swain, B. E.; Parsonage, D.; Hollis, T.; Harvey, S.; Perrino, F. W.; Kohli, R. M.; Taylor, E. W.; Hall, A. R. Solid-State Nanopore Analysis of Diverse DNA Base Modifications Using a Modular Enzymatic Labeling Process. *Nano Lett.* **2017**, *17* (11), 7110−7116.
(29) Sethi, K.; Dailey, G. P.; Zahid, O. K.; Taylor, E. W.; Ruzicka, J. A.; Hall, A. R. Direct Detection of Conserved Viral Sequences and Other Nucleic Acid Motifs with Solid-State Nanopores. *ACS Nano* **2021**, *15* (5), 8474−8483.
(30) Wadsworth, I. D.; Hall, A. R. Effects of Symmetric and Asymmetric Salt Conditions on a Selective Solid-State Nanopore Assay. *Nano Res.* **2022**, *15* (11), 9936−9942.
(31) Howarth, M.; Chinnapen, D. J.-F.; Gerrow, K.; Dorrestein, P. C.; Grandy, M. R.; Kelleher, N. L.; El-Husseini, A.; Ting, A. Y. A Monovalent Streptavidin with a Single Femtomolar Biotin Binding Site. *Nat. Methods* **2006**, *3* (4), 267−273.
(32) Fairhead, M.; Krndija, D.; Lowe, E. D.; Howarth, M. Plug-and-Play Pairing via Defined Divalent Streptavidins. *J. Mol. Biol.* **2014**, *426* (1), 199−214.
(33) Zahid, O. K.; Zhao, B. S.; He, C.; Hall, A. R. Quantifying Mammalian Genomic DNA Hydroxymethylcytosine Content Using Solid-State Nanopores. *Sci. Rep.* **2016**, *6* (1), 1−6.
(34) Zahid, O. K.; Rivas, F.; Wang, F.; Sethi, K.; Reiss, K.; Bearden, S.; Hall, A. R. Solid-State Nanopore Analysis of Human Genomic DNA Shows Unaltered Global 5-Hydroxymethylcytosine Content Associated with Early-Stage Breast Cancer. *Nanomedicine* **2021**, *35*, No. 102407.
(35) Yang, J.; Ferranti, D. C.; Stern, L. A.; Sanford, C. A.; Huang, J.; Ren, Z.; Qin, L.-C.; Hall, A. R. Rapid and Precise Scanning Helium Ion Microscope Milling of Solid-State Nanopores for Biomolecule Detection. *Nanotechnology* **2011**, *22* (28), No. 285310.
(36) Sriram, H.; Khanka, T.; Kedia, S.; Tyagi, P.; Ghogale, S.; Deshpande, N.; Chatterjee, G.; Rajpal, S.; Patkar, N. V.; Subramanian, P. G.; Gujral, S.; Hasan, S.; Tembhare, P. R. Improved Protocol for Plasma microRNA Extraction and Comparison of Commercial Kits. *Biochemia Medica* **2021**, *31* (3). 467.
(37) Luo, Y.; Wu, L.; Tu, J.; Lu, Z. Application of Solid-State Nanopore in Protein Detection. *Int. J. Mol. Sci.* **2020**, *21* (8), 2808.
(38) Fologea, D.; Gershow, M.; Ledden, B.; McNabb, D. S.; Golovchenko, J. A.; Li, J. Detecting Single Stranded DNA with a Solid State Nanopore. *Nano Lett.* **2005**, *5* (10), 1905−1909.
(39) Firnkes, M.; Pedone, D.; Knezevic, J.; Döblinger, M.; Rant, U. Electrically Facilitated Translocations of Proteins through Silicon Nitride Nanopores: Conjoint and Competitive Action of Diffusion, Electrophoresis, and Electroosmosis. *Nano Lett.* **2010**, *10* (6), 2162−2167.
(40) Lin, C.-T.; Loan, P. T. K.; Chen, T.-Y.; Liu, K.-K.; Chen, C.-H.; Wei, K.-H.; Li, L.-J. Label-Free Electrical Detection of DNA Hybridization on Graphene Using Hall Effect Measurements: Revisiting the Sensing Mechanism. *Adv. Funct. Mater.* **2013**, *23* (18), 2301−2307.
(41) Wilkins, M. R.; Gasteiger, E.; Bairoch, A.; Sanchez, J.-C.; Williams, K. L.; Appel, R. D.; Hochstrasser, D. F. Protein Identification and Analysis Tools in the ExPASy Server. In *2-D Proteome Analysis Protocols*; Link, A. J., Ed.; Methods in Molecular Biology; Humana Press: Totowa, NJ, 1999; pp 531−552. .
(42) Bjellqvist, B.; Hughes, G. J.; Pasquali, C.; Paquet, N.; Ravier, F.; Sanchez, J. C.; Frutiger, S.; Hochstrasser, D. The Focusing Positions of Polypeptides in Immobilized pH Gradients Can Be Predicted from Their Amino Acid Sequences. *Electrophoresis* **1993**, *14* (10), 1023−1031.
(43) Sivasankar, S.; Subramaniam, S.; Leckband, D. Direct Molecular Level Measurements of the Electrostatic Properties of a Protein Surface. *Proc. Natl. Acad. Sci. U. S. A.* **1998**, *95* (22), 12961−12966.
(44) Gao, T.; Zhang, W.; Wang, Y.; Yang, G. DNA Compaction and Charge Neutralization Regulated by Divalent Ions in Very Low pH Solution. *Polymers (Basel)* **2019**, *11* (2), 337.
(45) Wang, Y.-W.; Yang, G.-C. Modulation and Control of DNA Charge Inversion*. *Chinese Phys. B* **2017**, *26* (12), No. 128706.
(46) Hoogerheide, D. P.; Garaj, S.; Golovchenko, J. A. Probing Surface Charge Fluctuations with Solid-State Nanopores. *Phys. Rev. Lett.* **2009**, *102* (25), No. 256804.
(47) Wen, C.; Zeng, S.; Arstila, K.; Sajavaara, T.; Zhu, Y.; Zhang, Z.; Zhang, S.-L. Generalized Noise Study of Solid-State Nanopores at Low Frequencies. *ACS Sens* **2017**, *2* (2), 300−307.
(48) Carlsen, A. T.; Zahid, O. K.; Ruzicka, J.; Taylor, E. W.; Hall, A. R. Interpreting the Conductance Blockades of DNA Translocations through Solid-State Nanopores. *ACS Nano* **2014**, *8* (5), 4754−4760.
(49) Kowalczyk, S. W.; Wells, D. B.; Aksimentiev, A.; Dekker, C. Slowing down DNA Translocation through a Nanopore in Lithium Chloride. *Nano Lett.* **2012**, *12* (2), 1038−1044.
(50) He, Y.; Tsutsui, M.; Scheicher, R. H.; Fan, C.; Taniguchi, M.; Kawai, T. Mechanism of How Salt-Gradient-Induced Charges Affect the Translocation of DNA Molecules through a Nanopore. *Biophys. J.* **2013**, *105* (3), 776−782.
(51) Smeets, R. M. M.; Keyser, U. F.; Dekker, N. H.; Dekker, C. Noise in Solid-State Nanopores. *Proc. Natl. Acad. Sci. U. S. A.* **2008**, *105* (2), 417−421.

https://doi.org/10.1021/acssensors.4c00200
ACS Sens. XXXX, XXX, XXX−XXX

(52) Smeets, R. M. M.; Dekker, N. H.; Dekker, C. Low-Frequency Noise in Solid-State Nanopores. *Nanotechnology* **2009**, *20* (9), No. 095501.
(53) Wong, R. K. Y.; MacMahon, M.; Woodside, J. V.; Simpson, D. A. A Comparison of RNA Extraction and Sequencing Protocols for Detection of Small RNAs in Plasma. *BMC Genomics* **2019**, *20*, 446.
(54) de Gonzalo-Calvo, D.; Pérez-Boza, J.; Curado, J.; Devaux, Y. Challenges of microRNA-based Biomarkers in Clinical Application for Cardiovascular Diseases. *Clin Transl Med.* **2022**, *12* (2), No. e585.
(55) Kanagawa, T. Bias and Artifacts in Multitemplate Polymerase Chain Reactions (PCR). *J. Biosci Bioeng* **2003**, *96* (4), 317−323.

https://doi.org/10.1021/acssensors.4c00200
ACS Sens. XXXX, XXX, XXX−XXX